Biosensors and Bioelectronics 62 (2014) 343–349

Contents lists available at ScienceDirect

Biosensors and Bioelectronics

journal homepage: www.elsevier.com/locate/bios

Parallel recognition of cancer cells using an addressable array of solid-state micropores

Azhar Ilyas [a,b,c,1], Waseem Asghar [a,b,c,2], Young-tae Kim [c,d], Samir M. Iqbal [a,b,c,d,e,f,*]

[a] Nano-Bio Lab, University of Texas at Arlington, Arlington, TX 76019, USA
[b] Department of Electrical Engineering, University of Texas at Arlington, Arlington, TX 76011, USA
[c] Nanotechnology Research Center, University of Texas at Arlington, Arlington, TX 76019, USA
[d] Department of Bioengineering, University of Texas at Arlington, Arlington, TX 76010, USA
[e] Joint Graduate Committee of Bioengineering Program, University of Texas at Arlington and University of Texas Southwestern Medical Center at Dallas, University of Texas at Arlington, Arlington, TX 76010, USA
[f] Department of Urology, University of Texas Southwestern Medical Center at Dallas, Dallas, TX 75390, USA

ARTICLE INFO

Article history:
Received 16 April 2014
Received in revised form
20 June 2014
Accepted 24 June 2014
Available online 27 June 2014

Keywords:
CTC
Translocation profile
Pulse signal
Leukocytes
Detection efficiency
Single-cell measurement
Single-cell analysis

ABSTRACT

Early stage detection and precise quantification of circulating tumor cells (CTCs) in the peripheral blood of cancer patients are important for early diagnosis. Early diagnosis improves the effectiveness of the therapy and results in better prognosis. Several techniques have been used for CTC detection but are limited by their need for dye tagging, low throughput and lack of statistical reliability at single cell level. Solid-state micropores can characterize each cell in a sample providing interesting information about cellular populations. We report a multi-channel device which utilized solid-state micropores array assembly for simultaneous measurement of cell translocation. This increased the throughput of measurement and as the cells passed the micropores, tumor cells showed distinctive current blockade pulses, when compared to leukocytes. The ionic current across each micropore channel was continuously monitored and recorded. The measurement system not only increased throughput but also provided on-chip cross-relation. The whole blood was lysed to get rid of red blood cells, so the blood dilution was not needed. The approach facilitated faster processing of blood samples with tumor cell detection efficiency of about 70%. The design provided a simple and inexpensive method for rapid and reliable detection of tumor cells without any cell staining or surface functionalization. The device can also be used for high throughput electrophysiological analysis of other cell types.

1. Introduction

The shedding of tumor cells in peripheral blood was initially reported in 1889 (Paget, 1889). The circulating tumor cells (CTCs) are believed to detach from the primary tumor and spread through blood circulation or lymph nodes to secondary tissues (Kohn and Liotta, 1995). Patients with various types of cancers (breast, bladder, and renal) have been known to have CTCs in their peripheral blood (Cristofanilli et al., 2004; Lianidou and Markou, 2011; Loberg et al., 2004; Soria et al., 2002; Terstappen et al., 2000). Rapid recognition and accurate enumeration of CTCs in the peripheral blood can help in early diagnosis and to monitor the therapeutic efficiency. Reports show that number of CTCs can rise to 5000 CTCs per ml of blood in prostate cancer patients (Stott et al., 2010). But generally, CTCs are exceedingly low in number (1–200 cells per ml) which makes it very difficult to identify and quantify them from the whole blood at earlier stages of disease (Kahn et al., 2004; Krivacic et al., 2004; Nagrath et al., 2007; Rolle et al., 2005). Ultra-low concentration of CTCs in peripheral blood essentially calls for faster and efficient processing of blood sample.

The schemes employed for the isolation and quantification of CTCs include microfluidic flow cytometry, polycarbonate membrane filtration (size-based separation), chromatographic isolation and use of immunomagnetic systems (magnetic dynabeads) (Fu et al., 1999; Nagrath et al., 2007; Vona et al., 2000; Zabaglo et al., 2003). These techniques are limited by either low-throughput or the need for dye tags for cell quantification. Some of these strategies require expensive equipment and cannot be used as a point-of-care module (Adams et al., 2008; Zabaglo et al., 2003). Recently, Hosokawa et al. (2013) have reported a microcavity array

* Corresponding author at: Nano-Bio Lab, University of Texas at Arlington, 500 S. Cooper Street, Room #217, Arlington, TX 76019, USA. Tel.: +1 817 272 0228; fax: +1 817 272 7458.
E-mail address: smiqbal@uta.edu (S.M. Iqbal).
[1] Current address: Department of Biomedical Sciences, Texas A&M University, Baylor College of Dentistry, Dallas, TX 75246, USA.
[2] Current address: Department of Computer & Electrical Engineering and Computer Science, Florida Atlantic University, Boca Raton, FL 33431, USA.

http://dx.doi.org/10.1016/j.bios.2014.06.048
0956-5663/

system for size-based isolation and fluorescence-based quantification of CTCs from blood samples of advanced lung cancer patients. Though elegant, it also required fluorescent labeling for CTC enumeration. Solid-state micropores have been used for patch clamp measurements, electroporation, cell deformability examination and size based discrimination of cells (Matthews and Judy, 2006; Niu and Yan, 2001; ul Haque et al., 2009). The use of solid-state micropores in such a variety of applications owes it to their mechanical strength and thermal/chemical stability. Different techniques to drill micropores include deep reactive ion etching (DRIE), anisotropic etching of silicon, electrochemical etching and ion/electron beam sculpting (Li et al., 2001; Pantoja et al., 2004; Sugita et al., 2013). We have reported before a single solid-state micropore device for electrical detection of CTCs from whole blood (Asghar et al., 2012). Single channel detection faces a major challenge of high processing time. Here, we report a multi-channel device that utilizes multiple micropores for parallel recognition of tumor cells. As a model, an assay of two parallel micropores was used in a Teflon device assembly for simultaneous recording of ionic current flow across each of the two micropores. The device was able to detect tumor cells from the blood sample with 70% detection efficiency.

The CTCs are larger in size compared to other blood based cells and have different mechanical properties (Vona et al., 2000). Metastasis formulates them to be even more elastic since they need to squeeze through the surrounding tissues and enter the circulatory system (Ward et al., 1991; Wyckoff et al., 2000). Different morphology and biomechanical properties (size, shape, elasticity, viscosity, and stiffness) of tumor cells can be exploited to discriminate them from other cell types. The scheme reported here distinguishes the cancer cells from whole blood in a simple, inexpensive and speedy process that does not require any cell staining, surface functionalization or expensive equipment.

The cells were suspended in sodium chloride (0.85% w/v) solution and pushed under fluidic pressure. Separate Ag/AgCl electrode pairs were used to measure the ionic current across each micropore. Physical blockage of the micropore due to cell translocating through the micropore caused a drop in ionic current flow and an electrical pulse signal was recorded. The system was optimized for parallel recognition of cells and simultaneous recording of data without missing any translocation events. Tumor cells were identified by their characteristic pulse signals. Pulse magnitude, pulse duration and pulse shape were analyzed to recognize the cancer cells. This system can be applied to an automated and high throughput cellular analysis.

2. Materials and methods

2.1. Micropore device fabrication

All the chemicals were purchased from Sigma-Aldrich (St Louis, MO, USA) unless stated otherwise. The micropore fabrication process started with thermal oxidation of a double-side polished silicon wafer (100 orientation). The wafer was placed in the oxidation furnace to grow a 200 nm thick oxide layer on both sides of the wafer as shown in Fig. 1. After piranha cleaning, positive photoresist (Shipley S1813) was spin coated on one side of the Si wafer and conventional g-line photolightography was used to open square windows. Photoresist layer was manually applied to the other side (bottom) of the wafer to protect the oxide layer against buffered hydrofluoric (BHF) acid etch. The square window pattern was transferred to the underside oxide layer with BHF etch followed by removing all the remaining photoresist in acetone. Anisotropic etching of silicon was performed using diluted (25%) tetramethylammonium hydroxide (TMAH) which was maintained at 90 °C during the process. The silicon wafer was etched through the whole wafer thickness until TMAH reached the oxide layer on other side and gave 200 nm thick free-standing SiO_2 membranes. An optimized dose (30 kV acceleration voltage, 1 nA milling current, and 260 s exposure time) of focused ion beam (FIB) was

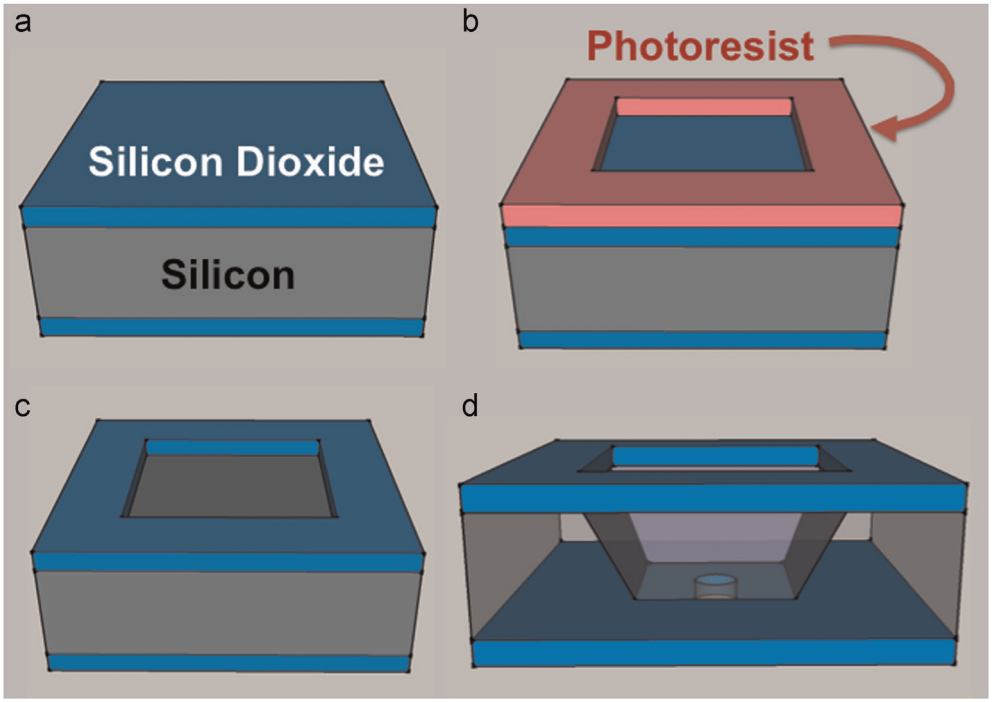

Fig. 1. Fabrication of solid-state micropores. (a) Thermally grown 200 nm thick oxide layer on both sides of double-side polished silicon wafer. (b) Photolithography to open square windows in the spin casted photoresist layer. (c) Transfer of square window pattern to the underlying oxide layer by BHF etch. (d) Anisotropic etch of silicon using TMAH which results in oxide membrane on the other side of the wafer (bottom side). FIB drills micropore in the membrane diaphragm.

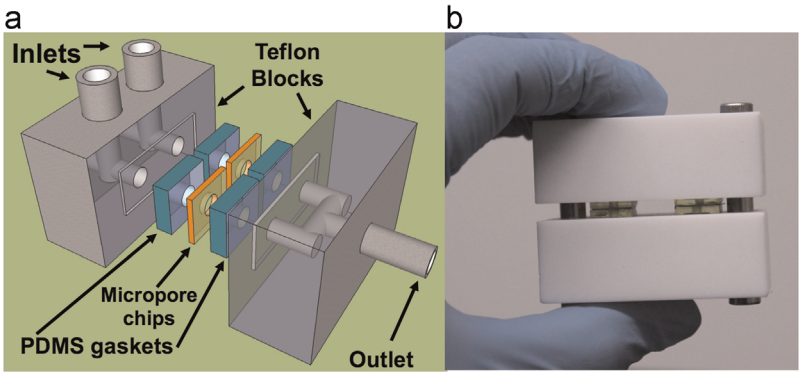

Fig. 2. Micropore array device assembly. (a) Cells are pushed into the Teflon block assembly at the inlets. The chips with micropores are sandwiched between the Teflon blocks. PDMS gaskets hold the micropore chips and avoid any leakage. Ag/AgCl electrodes are inserted in the tubing attached at the inlet and outlet compartments. (b) Assembled Teflon blocks show two parallel micropore devices sealed in PDMS gaskets.

used to drill 20 μm sized micropores in each of the 200 nm thick oxide membranes.

2.2. Device assembly for parallel processing

Two Teflon blocks (inlet, outlet) were used to sandwich the micropore chips. The inlet block had two channels each, ending in 1 mm holes. The outlet block also had two 1 mm openings which came together to form a single outlet chamber Fig. 2(a). The openings perfectly aligned together when the two blocks were assembled together. The device was designed to hold two individual micropore chips as an array of two instead of one chip with two micropores. First, aligning all the micropores on one chip against channel openings in the Teflon blocks would have been tedious unless special care was taken to drill the micropores at pre-defined positions on the membrane. Second, breakage/damage of a single membrane would have resulted in the loss of all micropores, whereas two chips with two micropores brought in inherent redundancy. One micropore on each chip made the design flexible and simple. Gaskets were made with polydimethylsiloxane (PDMS; Dow Corning) to hold chips on both sides to avoid any leakage of the solution as shown in Fig. 2(b). The inlet compartments of the Teflon block assembly were connected to a syringe pump (Harvard Apparatus) through tubing adapters. Cells, suspended in sodium chloride solution, were injected into the inlet compartments at optimal flow rate using the syringe pump whereas the outlet compartment was initially filled with sodium chloride solution. Ag/AgCl electrodes were dipped in the NaCl solution to measure the ionic current flow across the micropores. Data acquisition cards (National Instruments) were connected to these electrodes for providing voltage bias and recording ionic current measurements. Physical blockage of the micropore during cell translocation increased the resistance to the flow of ions across the micropore and consequently a corresponding resistive pulse signal was observed.

2.3. Human derived primary renal cancer cells collection and culture

Human primary renal cancer cells metastasized to human brain were isolated from a consenting patient at the University of Texas Southwestern Medical Center at Dallas (TX, USA) with the approval of Institutional Review Board (IRB). Ice-cold Hank's medium was used to collect the brain tissue containing metastatic tumor cells which were chemically dissociated with papain (2%) and dispase (2%) as reported previously (Marin-Valencia et al., 2012). The cells were cultured with Dulbecco's modified Eagle's medium (DMEM) supplemented with 10% fetal bovine serum. The cultured cells were enzymatically dissociated with trypsin (0.25%)–EDTA (0.03%) solution to obtain the cells for the experiments. These cells were spiked in blood samples before the experiments.

2.4. Red blood cell lysis using lysis buffer

The red blood cell (RBC) lysis buffer was purchased from eBioscience (CA, USA). A volume of 10 ml of the 1 × lysis buffer was added to 1 ml of whole blood and the solution was incubated for 10 min. The lysis buffer was then diluted by adding 20–30 ml of 1 × PBS to stop the lysing reaction. After that, the solution was centrifuged at 300–400*g* to collect the cells at the bottom of the tube in the form of the a pellet. The pellet was resuspended in NaCl solution for cell processing. A small volume was observed under microscope to confirm that there were no RBCs left. Standard cell counting with a hemocytometer also confirmed about 1000 time reduction in cell density. Though the pellet collected after lysis contained only white blood cells (WBCs), a very few residual RBCs were also observed. Since RBCs are smaller than WBCs, these would not affect cancer cell identification. However, if needed, a second round of lysis could have been performed. Polypropylene cell strainer (BD Falcon) with a nylon mesh of 100 μm size was used before processing to remove any chunks or cell clumps and to ensure single cell suspension in the investigated sample.

3. Results and discussion

The scanning electron microscope (SEM) analysis confirmed the anisotropic etching of silicon using TMAH etch. The bulk silicon was etched at an angle of 54.7° making slanted sidewalls which ended at free-standing oxide membrane as shown in Fig. 3 (a). The diameter of the drilled micropore was controlled by the FIB parameters (acceleration voltage, beam current and drilling time) and beam size. Membrane material and the thickness of the membrane also affected the diameter of the micropore (Asghar et al., 2011a, 2011b). Higher dose gave a larger pore for oxide membranes of similar thickness. SEM analysis showed that inner periphery of the micropore was not smooth and could rupture the cell membrane when these would translocate through the micropore. Second, crimped topography of membrane revealed the residual stress in the oxide membrane. Therefore, the SiO_2 membranes were annealed at 1050 °C for 5 min. Thermal treatment made the inner walls of the micropore smoother and reduced the residual stress of the membrane. Fig. 3(b) shows SEM micrograph of a micropore after thermal treatment.

The cultured cells were trypsinized and suspended in NaCl solution for parallel processing with multi-channel framework. All

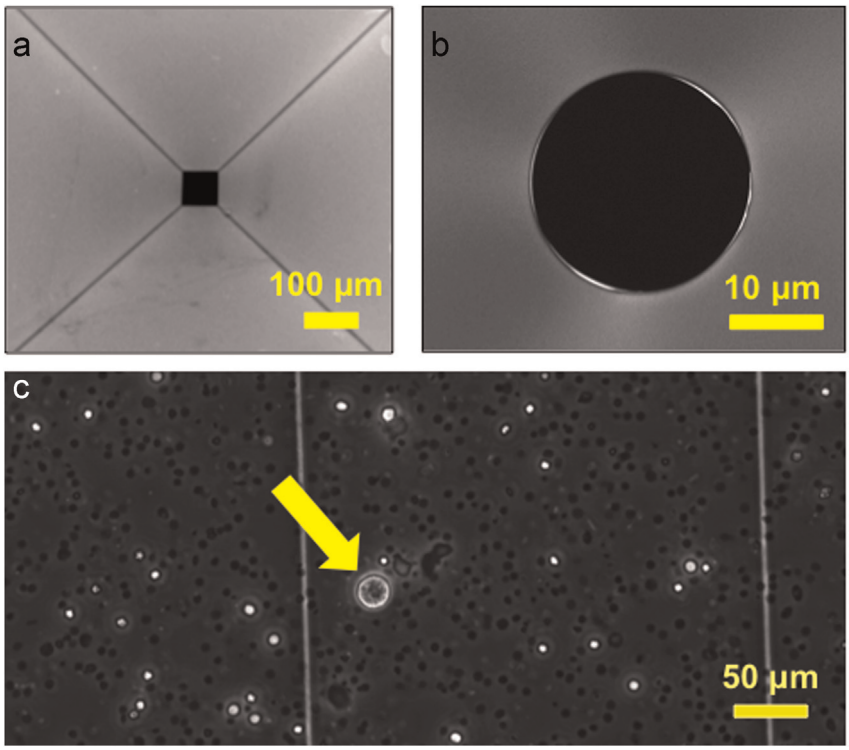

Fig. 3. Micropore fabrication and cell suspension. (a) SEM micrograph shows slanted sidewalls in bulk silicon ending at oxide membrane (center) after TMAH etch. (b) SEM micrograph of a micropore drilled in the oxide membrane after thermal annealing. (c) Optical micrograph shows that renal cancer cells (pointed by arrow) are larger in size than WBCs. The disaggregated cells are seen to be healthy and hold spherical shape in suspension.

the disaggregated cells held spherical shape in suspension and were found healthy after trypsinization. Trypan Blue exclusion dye (0.4%) was used to assess the viability of the cells and measurements on hemocytometer showed that more than 94% of dissociated cells were viable. The optical micrograph for the mixed cell suspension is shown in Fig. 3(c), which reveals that human primary renal cancer cells (pointed by arrow) are much larger in size (average diameter ~30 μm) compared to the white blood cells (WBCs).

Multi-channel micropores were assembled as explained in Section 2. Micropore diameter, membrane thickness, flow rate and sampling frequency were critical parameters to optimize for the best translocation data. Translocation profile of cells significantly changed if any of these parameters varied (except membrane thickness). When a cell translocated through the micropore, physical blockage of the micropore reduced the conductivity of the micropore by offering more resistance to the flow of ionic current. Resistance to the flow of current is given by $R=\rho L/A$ where ρ is the resistivity of NaCl (0.85% w/v) solution, L denotes the thickness of oxide membrane (length of the micropore) and A represents the effective area of the micropore. Therefore, physical blockage of the micropore altered the effective area which consequently changed the resistance across the micropore and a drop in ionic current was recorded for every translocating cell. Since the drop in current (amplitude) and the time taken by the cell to pass through the micropore (pulse width) were strongly coupled with the biomechanical (size, shape, and stiffness) properties of the cell, characteristic pulse signals were observed for each cell type. Both the channels showed similar translocation profiles for specific cell types as shown in Fig. 4. As explained above, the pulse frequency represents the cell concentration and can be used for cell counting. A high concentration (10k cells per ml) and a low concentration (100 cells per ml) of human primary renal cancer cells were suspended separately in NaCl solution. The samples were processed separately for 30 min using the multi-channel device at optimized settings. The number of pulses reflected the cell concentration which illustrated the capability of the device to quantify the cancer cells (Fig. 4(b)). It also showed high sensitivity of the device demonstrated by detecting a very low concentration of cells. The translocation profile was found to be steady regardless of the cell concentration or the time (Fig. 4(c)). It validated the consistency and reliability of the device for long measurements.

The key objective of parallel recognition was to increase the throughput by rapid processing of blood samples. The exposure to lysis buffer reduced the cell concentration per ml of blood by three orders of magnitude which eliminated the need for blood dilution. In other works, the whole blood has to be diluted as much as 10 times to avoid blockage/clogging of micropore (Asghar et al., 2012). Dilution raised the sample volume by 10 times and furthermore single micropore measurements made it a very low throughput system. The array scheme made it a rapid processing device. Moreover, cells collected from 1 ml of blood were resuspended in 500 μl of NaCl solution which reduced the sample volume by half while keeping the cell density still low enough to be processed by the device without getting blocked. Thus, just by adding one extra channel, the throughput increased by 40 times. At optimized flow rate, it took only 25 min to process 1 ml of blood.

The metastatic renal cancer cells gave distinctive current blockage statistics. As already mentioned, WBCs were smaller in size so these offered lesser physical blockage to the micropore which showed different translocation profiles. The experiments were repeated at least three times and similar results were observed. The pulse characteristics (pulse width, peak amplitude) showed that cancer cells were easily identifiable as can be seen in Fig. 5(a) which displays the two scatter plots combined; one for pulse distributions for cell suspensions containing only cancerous cells and the second for only WBCs. The cell suspensions for two cell types were processed separately and the distributions of electrical profiles are drawn on the same plot to have a clear view

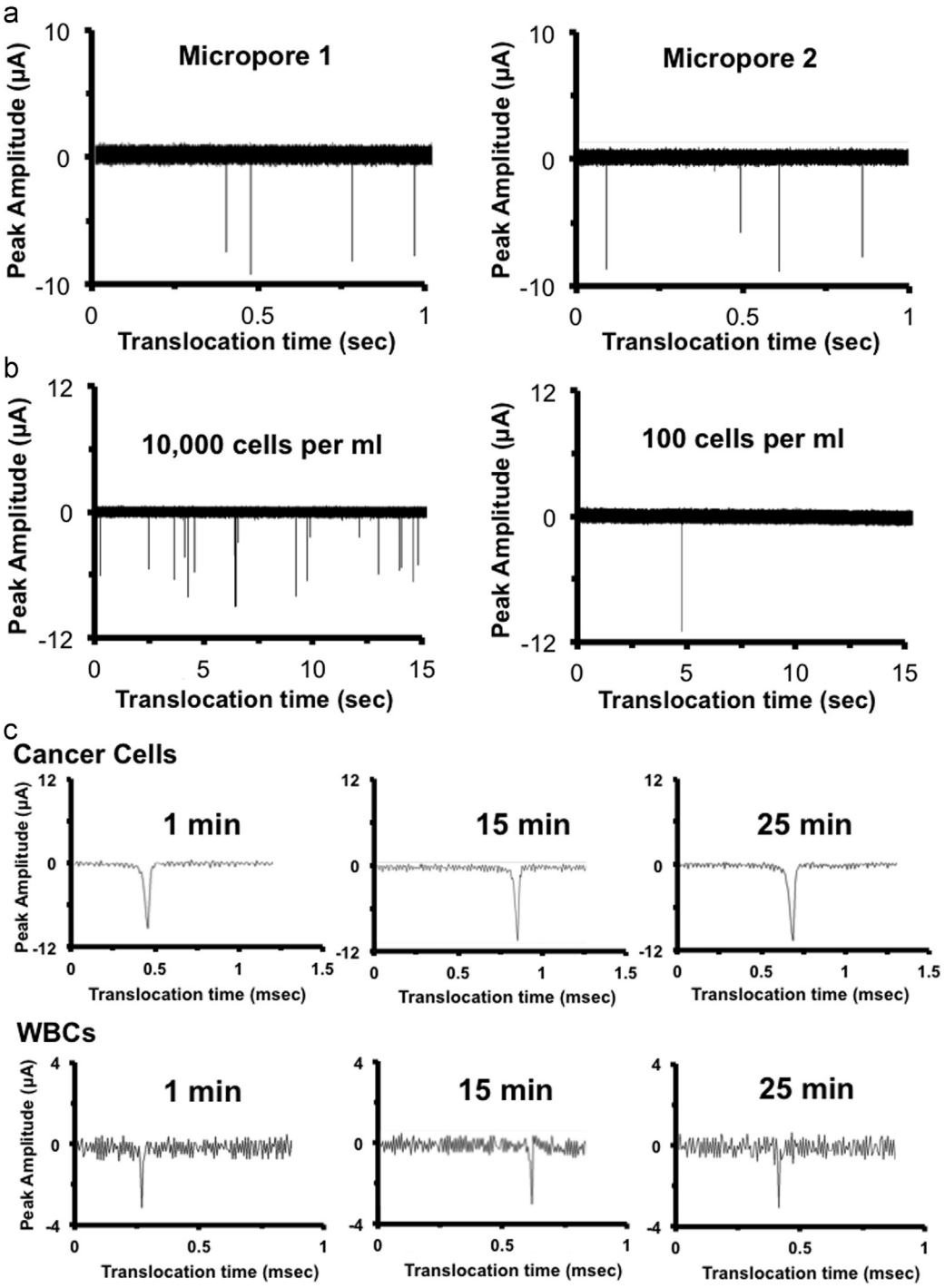

Fig. 4. Reliability and cell enumeration. (a) Micropore 1 and micropore 2 show similar electrical signal for cancer cells during simultaneous recording of data across each of them. Frequency of pulses reflects the number of translocated cells. Similar pulse frequency demonstrates uniform distribution of cells across each channel. (b) Comparison of the current signal for high concentration and low concentration of cell suspension reveals that the number of pulses reflects the cell concentration and can be used for cell counting. (c) The device shows similar electronic signatures at 1, 15 and 25 min after first cell detection. A stable and consistent translocation profile for both cell types throughout the experiments indicates the reliability of the device.

of the location of cancer cells on the plot. It helped us to determine the width of pulse distribution for cancer cells, shown by the dotted ovals in Fig. 6. More than 95% of cancer cells show distinctive translocation profile from WBCs owing to their different biomechanical properties.

The pulse signals from cells clumped together could easily be discriminated from single cell pulses. Clumps resulted in pulses that had double or triple dips at the bottom of the pulse as shown in Fig. 5(d). Since the scope of the study was to distinguish cancer cells from normal blood cells based upon electronic signatures from single cells, the clumped cells data was ignored and comparison was done only between the electrical profiles of single cells.

The characteristic pulse signals are shown closely in Fig. 5 (b) and (c). The pulse statistics for both types of cells are given in Table 1 which shows the average values of translocation time and peak amplitude for thousands of cells. The analysis of data based

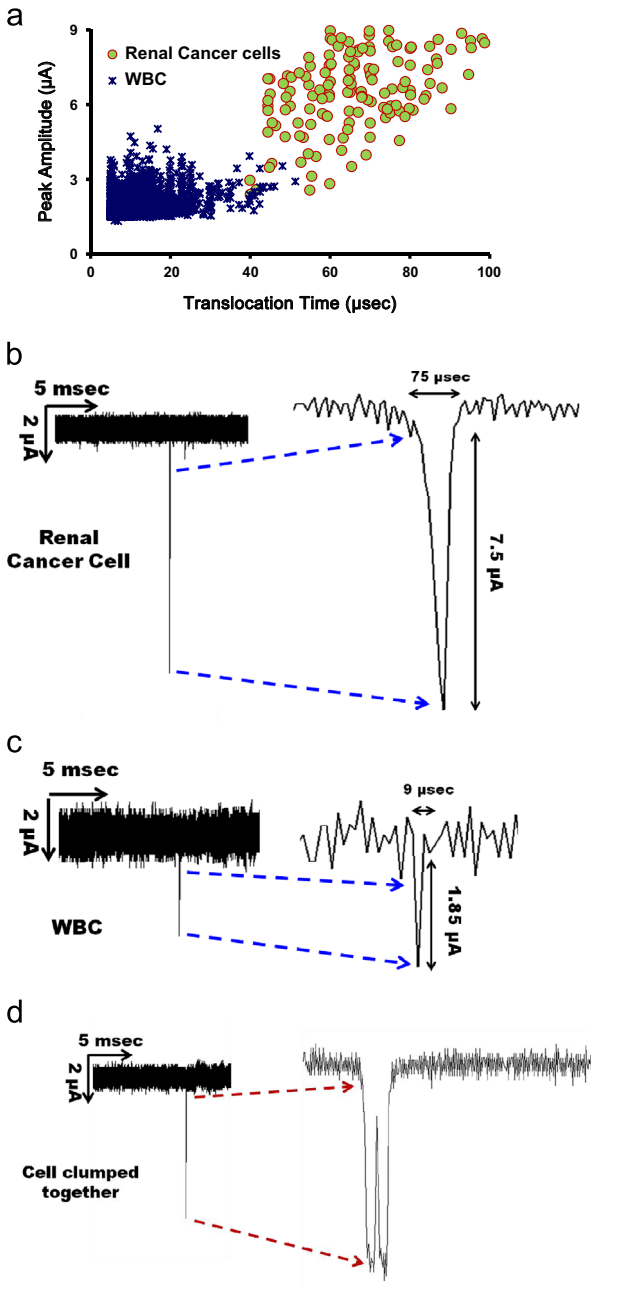

Fig. 5. Scatter plot and translocation current trace for the cells passing through the micropore. (a) The distribution of pulses for both types of cells processed separately through the multi-channel micropore device is shown on a single plot for comparison. The scatter plot shows clearly separate data distribution for cancer cells as compared to white blood cells (WBCs). (b) and (c) Characteristic translocation profile (translocation time, current peak amplitude) for renal cancer cells and WBCs respectively. (d) The pulse shape shows that the signal is from the cells clumped together. This information is used to exclude these data points from analysis.

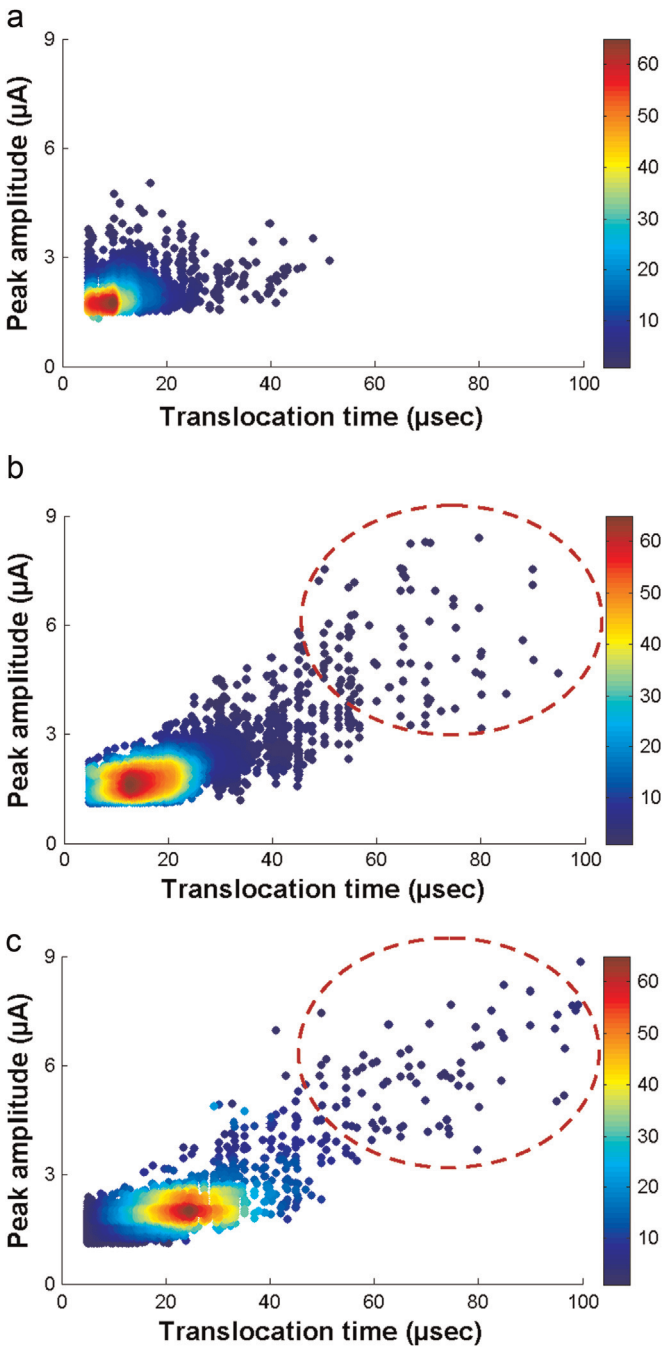

Fig. 6. Data density plots for mixed cell suspension. Scatter plots for freshly collected (a) rat blood (without cancer cells) shows distribution of pulse signals for WBCs. The color-map on the right indicates the data density distribution of cells. Cancer cells spiked in freshly collected (b) rat blood and (c) human whole blood demonstrate that characteristic current signal discriminates cancer cells from WBCs and can be efficiently recognized out of a mixed cell suspension as pointed out by the dashed ovals. (For interpretation of the references to color in this figure legend, the reader is referred to the web version of this article.)

on translocation time and peak amplitude was carried out using one-way ANOVA for independent samples which showed that the two types were significantly different from each other (p-value < 0.001). The pulse shape also provided further information about the translocating cell. The orientation of the cell and its biomechanical properties predominately defined the pulse characteristics and pulse shape (Asghar et al., 2012; Chen et al., 2004). The ionic current value corresponded to a cross-sectional circular contour which indicated the physical dimension of the translocating cell. Thus, the data could be used to accurately track 3D electrical profile of the translocating cell at optimized settings of the measurement system. Moreover, the slope of the pulse signal indicated the stiffness of the translocating cell which can be used to study the biomechanical properties of the investigated cells.

After defining the signature pulse signals for renal cancer cells and the WBCs, a mixture of renal cancer cells and freshly collected whole blood samples (human and rat) were investigated to determine the detection efficiency of our device from mixed cell suspension. One hundred renal cancer cells were spiked in 1 ml of

Table 1
Pulse statistics for both cell types through 20 μm micropore 1 and micropore 2.

Cell types	Measurement (units)			
	Average translocation time (μs)		Average peak amplitude (μA)	
	μpore **1**	μpore **2**	μpore **1**	μpore **2**
Renal cancer cells	73.50 ± 18.13	78.37 ± 36.30	7.52 ± 3.44	7.69 ± 2.83
WBCs after RBC lysis	9.60 ± 6.02	9.18 ± 5.64	1.83 ± 0.47	1.84 ± 0.40

whole blood and RBC lysis buffer was used to get rid of RBCs (as explained in Section 2.4). The solution was centrifuged and the collected pellet was resuspended in NaCl solution to get a mixed cell suspension as shown in Fig. 6. Trypan Blue assay confirmed the viability of cancer cells in mixed suspension which showed that RBC lysis did not affect the cancer cells present in the blood sample. The cancer cells were spiked in freshly collected blood samples from human and rat. Both types of blood samples were processed separately under similar conditions. The data demonstrated that cancer cells were easily distinguished from WBCs even when these were mixed at very low concentration (100 cells per ml) as shown by the density plots in Fig. 6. The color variation indicates the density of data points and dashed ovals point out the region characteristic of the translocation profiles of cancer cells determined from the scatter plot given in Fig. 5(a). The data showed that more than 70% of cancer cells spiked in whole blood gave electrical profiles specific to cancer cells and were easily identified by the distribution of these pulses in the elliptical area defined for cancer cells. Thus, the multichannel micropore system provided statistical analysis on single cell level and used electronic fingerprints of cancer cells to discriminate them from WBCs with 70% detection efficiency in a high throughput fashion.

4. Conclusions

A rapid scheme to detect cancer cells from whole blood using a solid-state micropore array is reported. An array of micropores with simultaneous recording data for parallel recognition of cancer cells resolved the key challenge of the throughput for single solid-state micropore devices. The cells were pushed under optimized fluid pressure to record electronic signatures for one cell at a time. The biophysical properties of cells gave characteristic pulse signals which discriminated the cancer cells from other cell types. The multi-channel micropore device did not need any cell staining, surface functionalization or expensive equipment. It not only efficiently detected the cancer cells but also provided statistical contribution from pulses of every single cell in a high throughput fashion. The throughput and processing can be increased by easily adding more micropores in the array. The system is also capable of investigating other samples where biomechanical properties of cells can be used as the discriminating factor to indicate the physiological status of the cells.

Acknowledgments

The authors would like to thank C.M.A. Arafat for help with LabView and M.R. Hasan for assistance with the graphics. The work was supported by grant from the National Science Foundation (ECCS-1201878) to S.M. Iqbal. Azhar Ilyas acknowledges support from the Cancer Research Foundation of North Texas, Arlington, Texas, USA.

References

Adams, A.A., Okagbare, P.I., Feng, J., Hupert, M.L., Patterson, D., Gottert, J., McCarley, R.L., Nikitopoulos, D., Murphy, M.C., Soper, S.A., 2008. J. Am. Chem. Soc. 130, 8633–8641.
Asghar, W., Ilyas, A., Billo, J.A., Iqbal, S.M., 2011a. Nanoscale Res. Lett. 6, 1–6.
Asghar, W., Ilyas, A., Deshmukh, R.R., Sumitsawan, S., Timmons, R.B., Iqbal, S.M., 2011b. Nanotechnology 22, 285304.
Asghar, W., Wan, Y., Ilyas, A., Bachoo, R., Kim, Y., Iqbal, S.M., 2012. Lab Chip 12, 2345–2352.
Chen, P., Gu, J., Brandin, E., Kim, Y.-R., Wang, Q., Branton, D., 2004. Nano Lett. 4, 2293–2298.
Cristofanilli, M., Budd, G.T., Ellis, M.J., Stopeck, A., Matera, J., Miller, M.C., Reuben, J. M., Doyle, G.V., Allard, W.J., Terstappen, L.W.M.M., 2004. N. Engl. J. Med. 351, 781–791.
Fu, A.Y., Spence, C., Scherer, A., Arnold, F.H., Quake, S.R., 1999. Nat. Biotechnol. 17, 1109–1111.
Hosokawa, M., Kenmotsu, H., Koh, Y., Yoshino, T., Yoshikawa, T., Naito, T., Takahashi, T., Murakami, H., Nakamura, Y., Tsuya, A., 2013. PloS One 8, e67466.
Kahn, H.J., Presta, A., Yang, L.-Y., Blondal, J., Trudeau, M., Lickley, L., Holloway, C., McCready, D.R., Maclean, D., Marks, A., 2004. Breast Cancer Res. Treat. 86, 237–247.
Kohn, E.C., Liotta, L.A., 1995. Cancer Res. 55, 1856–1862.
Krivacic, R.T., Ladanyi, A., Curry, D.N., Hsieh, H.B., Kuhn, P., Bergsrud, D.E., Kepros, J. F., Barbera, T., Ho, M.Y., Chen, L.B., 2004. Proc. Natl. Acad. Sci. U. S. A. 101, 10501–10504.
Li, J., Stein, D., McMullan, C., Branton, D., Aziz, M.J., Golovchenko, J.A., 2001. Nature 412, 166–169.
Lianidou, E.S., Markou, A., 2011. Clin. Chem. 57, 1242–1255.
Loberg, R.D., Fridman, Y., Pienta, B.A., Keller, E.T., McCauley, L.K., Taichman, R.S., Pienta, K.J., 2004. Neoplasia 6, 302.
Marin-Valencia, I., Cho, S.K., Rakheja, D., Hatanpaa, K.J., Kapur, P., Mashimo, T., Jindal, A., Vemireddy, V., Good, L.B., Raisanen, J., Sun, X., Mickey, B., Choi, C., Takahashi, M., Togao, O., Pascual, J.M., DeBerardinis, R.J., Maher, E.A., Malloy, C. R., Bachoo, R.M., 2012. NMR Biomed. 25, 1177–1186.
Matthews, B., Judy, J.W., 2006. J. Microelectromech. Syst. 15, 214–222.
Nagrath, S., Sequist, L.V., Maheswaran, S., Bell, D.W., Irimia, D., Ulkus, L., Smith, M.R., Kwak, E.L., Digumarthy, S., Muzikansky, A., 2007. Nature 450, 1235–1239.
Niu, X., Yan, Z., 2001. J. Biomed. Eng. 18, 615.
Paget, S., 1889. Lancet 133, 571–573.
Pantoja, R., Nagarah, J.M., Starace, D.M., Melosh, N.A., Blunck, R., Bezanilla, F., Heath, J.R., 2004. Biosens. Bioelectron. 20, 509–517.
Rolle, A., Gunzel, R., Pachmann, U., Willen, B., Hoffken, K., Pachmann, K., 2005. World J. Surg. Oncol. 3, 18.
Soria, J.-C., Morat, L., Durdux, C., Housset, M., Cortez, A., Blaise, R., Sabatier, L., 2002. J. Urol. 167, 352–356.
Stott, S.L., Lee, R.J., Nagrath, S., Yu, M., Miyamoto, D.T., Ulkus, L., Inserra, E.J., Ulman, M., Springer, S., Nakamura, Z., 2010. Sci. Transl. Med. 2. (25-23).
Sugita, T., Hiramatsu, K., Ikeda, S., Matsumura, M., 2013. ACS Appl. Mater. Interfaces 5, 2580–2584.
Terstappen, L.W., Rao, C., Gross, S., Weiss, A.J., 2000. Int. J. Oncol. 17, 573–581.
ul Haque, A., Zuberi, M., Diaz-Rivera, R.E., Porterfield, D.M., 2009. Biomed. Microdevices 11, 1239–1250.
Vona, G., Sabile, A., Louha, M., Sitruk, V., Romana, S., Schütze, K., Capron, F., Franco, D., Pazzagli, M., Vekemans, M., 2000. Am. J. Pathol. 156, 57–63.
Ward, K.A., Li, W.I., Zimmer, S., Davis, T., 1991. Biorheology 28, 301.
Wyckoff, J.B., Jones, J.G., Condeelis, J.S., Segall, J.E., 2000. Cancer Res. 60, 2504–2511.
Zabaglo, L., Ormerod, M.G., Parton, M., Ring, A., Smith, I.E., Dowsett, M., 2003. Cytometry Part A 55, 102–108.